Air-sea interface in hurricane conditions

Alexander Soloviev,[1,2] Atsushi Fujimura,[2] and Silvia Matt[1]

Received 15 November 2011; revised 5 August 2012; accepted 6 September 2012; published 18 October 2012.

[1] Improving hurricane prediction models requires better understanding of complex processes taking place at the air-sea interface at high wind speeds. The change of the air-sea interaction regime in hurricane conditions has been linked to the mechanism of direct disruption of the air-sea interface by pressure fluctuations working against the surface tension force. This can be achieved through the Kelvin-Helmholtz type instability. In order to investigate this mechanism, we have conducted a series of 3D numerical experiments using a volume of fluid multiphase model. The experiments were initialized with either a flat interface or short wavelets and wind stress applied at the upper boundary of the air layer. The direct disruption of the air-water interface and formation of two-phase transition layer were observed in the numerical model under hurricane force wind. The vertical profiles of density and velocity in the transition layer were consistent with the regime of marginal stability, which permitted estimation of the lower limit on the drag coefficient under hurricane conditions. This limit was appreciably lower than the wave resistance law; though, it was gradually increasing with wind speed. The numerical experiments with imposed short wavelets demonstrated the tearing of wave crests, formation of water sheets and spume ejected into the air, smoothing of the water surface, as well as quasiperiodic structures on the top of wave crests resembling the Tollmien-Schlichting instability. This study can help in developing a framework for combining the effects of the two-phase environment with the contribution to the drag from waves.

Citation: Soloviev, A., A. Fujimura, and S. Matt (2012), Air-sea interface in hurricane conditions, *J. Geophys. Res.*, *117*, C00J34, doi:10.1029/2011JC007760.

1. Introduction

[2] Improving numerical weather prediction tropical cyclone models requires a better understanding of complex processes taking place in the oceanic and atmospheric boundary layers at very high wind speeds. The role of sea spray in this process is not yet completely understood. Estimates provided by *Soloviev and Lukas* [2006] and *Ingel'* [2010] suggest that, in the framework of existing sea spray generation functions [e.g., *Andreas*, 1998], the reduction of turbulent friction due to buoyancy effects associated with the entrainment of spray droplets in the airflow has a relatively small effect on the drag coefficient when referred to a standard 10 m height. Furthermore, the wind loses a part of its momentum to accelerate the spray, which should result in a slow increase of the drag coefficient with wind speed rather than its decrease.

[3] Contribution of waves and inertial currents can significantly influence the air-sea drag coefficient and momentum exchange in hurricanes [*Kukulka et al.*, 2007; *Kukulka and Hara*, 2008; *Fan et al.*, 2009]. Surface waves are also a source of turbulence in the upper ocean [*Wang and Qiao*, 2008; *Babanin and Haus*, 2009; *Qiao et al.*, 2010]. However, our work is focused on the estimation of the effect of the two-phase environment at the air-sea interface on the drag coefficient. Merging this parameterization with the wave parameterizations is the subject of future work.

[4] In this paper, we further develop the hypothesis formulated by *Soloviev and Lukas* [2006] that the change of the air-sea interaction regime in hurricane conditions is associated with the mechanism of breakup of the interface into droplets or spray. In his laboratory experiment, *Koga* [1981] observed the direct disruption of the air-water interface by pressure fluctuations working against surface tension, accompanied by intense generation of large spray particles - spume. Direct disruption of the interface between air and water can be achieved through the Kelvin-Helmholtz (KH) instability of the interface. In addition, the Tollmien-Schlichting (TS) instability of viscous sublayers from the air and/or water side is potentially another important process taking place at the air-sea interface under hurricane conditions. Similar processes take place at the atomization of liquid fuels in cryogenic and diesel engines [*Yecko et al.*, 2002]. Under hurricane conditions, such instabilities initiate the tearing of short wavelet

[1]Oceanographic Center, Nova Southeastern University, Dania Beach, Florida, USA.
[2]Rosenstiel School of Marine and Atmospheric Science, University of Miami, Miami, Florida, USA.

Corresponding author: A. Soloviev, Oceanographic Center, Nova Southeastern University, 8000 N. Ocean Dr., Dania Beach, FL 33004, USA. (soloviev@nova.edu)

0148-0227/12/2011JC007760

crests, ejection of spume, and smoothing of the sea surface, which reduces the drag coefficient at the air-sea interface, an effect observed in the field and laboratory experiments [*Powell et al.*, 2003; *Donelan et al.*, 2004; *Black et al.*, 2007; *Troitskaya et al.*, 2010].

[5] The outline of this paper is as follows. Section 2 presents the conceptual framework for this work. Section 3 describes the numerical model of the air-sea interface implemented with computational fluid dynamics (CFD). Section 4 presents results of numerical simulations of the effect of direct disruption of the air-sea interface in hurricane conditions. In Section 5, we discuss the application of the numerical model results to the parameterization of the lower limit on the air-sea drag coefficient under hurricane conditions. In Section 6, we reproduce tearing of wave crests, which leads to the smoothing of the sea surface. Section 7 is the discussion and conclusions.

2. Conceptual Framework

[6] A non-dimensional number

$$K = u_{*a}/\left(g\sigma_s\rho_w/{\rho_a}^2\right)^{1/4} \tag{1}$$

has been proposed as the criteria for the direct disruption of the air-sea interface and called the Koga number by *Soloviev and Lukas* [2010]. The instability occurs at $K > K_{cr}$, where $K_{cr} \approx 0.26$ (corresponding to $U_{10} \approx 30$ m s^{-1}). In this formula u_{*a} is the friction velocity from the air side, g is the acceleration due to gravity, σ_s is the surface tension, ρ_w and ρ_a are the water and air density, respectively.

[7] When the Koga number exceeds its critical value, the KH type instability is able to break up the air-sea interface. As a result, a two-phase transition layer is formed. *Soloviev and Lukas* [2006] concluded that this transition layer maintains the regime of marginal stability.

[8] *Soloviev and Lukas* [2010] applied the *Miles and Howard* [1964] and *Cushman-Roisin* [1994] linear theory to derive the necessary condition for the instability of the two-phase transition layer at the air-sea interface as follows:

$$gH\left(\rho_w^2 - \rho_a^2\right) < m\rho_a\rho_w\Delta U^2 \tag{2}$$

where $\Delta U = U_w - U_a$ is the velocity difference across the transition layer, ρ_w and ρ_a are bulk densities for water and air; U_a and U_w are velocities for water and air at the lower and upper boundaries of transition layer, respectively; and

$$m \approx 1. \tag{3}$$

Equation (2) is also based on the *Lefebvre* [1989] and *Lasheras and Hopfinger* [2000] theory that the subsequent nonlinear development of the instability is likely to be related to the initial linear instability.

[9] Note that the surface tension, which is a determining parameter in the formulation for the Koga number, does not enter equation (2). After the disruption of the sea surface and formation of the transitional layer, surface tension is no longer a relevant parameter because the clearly defined interface does not exist. The surface tension effects are still important for air bubbles and spray droplets constituting the transition layer (though at the smaller-size end of their size spectra only).

[10] Equation (2) can then be expressed in the following way:

$$Ri_* < mRi_{cr} \tag{4}$$

where

$$Ri_* = gH\left(\rho_w^2 - \rho_a^2\right)/\left(2\rho_w\rho_a\,\Delta U^2\right) \approx gH\rho_w/\left(2\rho_a\Delta U^2\right) \tag{5}$$

is the global Richardson number defined for large density differences between the layers, and $Ri_{cr} = 1/2$ is the critical value of Ri following from (2)–(5).

[11] Remarkably, for small density differences between the layers and small depth increments dz, Ri_* defined via equation (6) transforms into the classic gradient Richardson number,

$$Ri = (g/\rho)(\partial\rho/\partial z)/\left[(\partial u/dz)^2 + (\partial v/\partial z)^2\right], \tag{6}$$

where ρ is the average density, and u and v the average horizontal velocity components.

[12] As mentioned above, for a two-layer system with large density difference, it follows from equations (4)–(6) that $Ri_{cr} = 1/2$. The theoretical analysis by *Cushman-Roisin* [1994] and *Cushman-Roisin and Beckers* [2011] for the two layer system including a transition layer with linear profiles of velocity and relatively small density difference (Boussinesq approximation), resulted in $Ri_{cr} = 1/4$. Based on a comment in *Cushman-Roisin* [1994], *Gramer* [2007] hypothesized that the difference in Ri_{cr} between discontinuous and linear density and velocity profiles is due to consumption of kinetic energy by vertical motions for the case of a continuous environment. This is also consistent with the fact that $Ri_{cr} = 1/2$ refers to the onset of the instability, while $Ri_{cr} = 1/4$, to complete, three-dimensional mixing.

[13] The two-phase transition layer developing under hurricane conditions at the air-sea interface has a very large density difference across. As a result, the Boussinesq approximation is no longer valid in this case. Furthermore, the strong density stratification effectively suppresses the vertical velocity component and the system may still dynamically resemble an interface. Consequently, one can expect that the critical value of the Richardson number defined by equation (6) will be closer to 1/2 rather than 1/4.

[14] The thickness of the transition layer can be estimated from equation (5) and condition $Ri_* = mRi_{cr}$ as follows:

$$H = 2mRi_{cr}\Delta U^2\rho_a\rho_w\left(\rho_w^2 - \rho_a^2\right)^{-1}g^{-1} \approx 2mRi_{cr}\Delta U^2\rho_a{\rho_w}^{-1}g^{-1}, \tag{7}$$

where ΔU is the velocity difference across the transition layer.

[15] Observations of the air-sea interface in hurricane conditions are difficult and data are very limited [*Powell et al.*, 2003; *Black et al.*, 2007]. In order to investigate the mechanism of the breakup of the air-sea interface and dynamics of the two-phase transition layer, we have

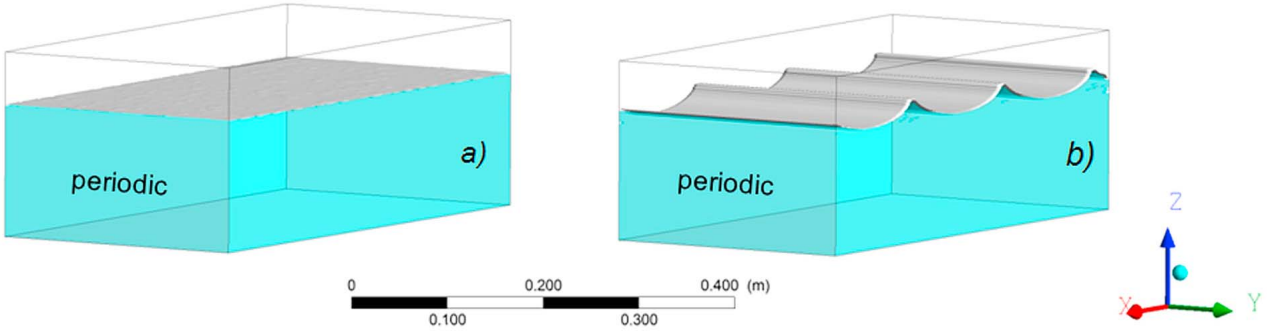

Figure 1. Initial conditions for two cases: (a) flat air-water interface and (b) short waves of 0.33 m wavelength imposed.

conducted and described in this paper a series of numerical experiments using the CFD software ANSYS Fluent [*ANSYS, Inc.*, 2009].

3. Numerical Model

3.1. Model Settings

[16] The domain for the simulations was 1 m by 0.5 m in the horizontal, by 0.35 m in the vertical. The air layer had a thickness of 0.1 m, with a 0.25 m thick water layer in the bottom part of the domain. The horizontal grid spacing was 5 mm, the vertical spacing was 1 mm at the interface with a growth rate of 1.1 until 5 mm was reached, and then held constant. The resolution was increased for the case initialized with wavelets, where the vertical grid spacing was kept at 1 mm to within 20 mm of the surface, then increased with a growth rate of 1.1. The total number of cells in the domain was approximately 2 million.

[17] The numerical experiments were initialized with either a flat interface (Figure 1a) or short wavelets (Figure 1b). Wind stress was applied at the upper boundary of the air layer, ranging from zero stress to hurricane force stress. Periodic boundary conditions were applied along the x-direction and zero shear conditions were chosen on lateral sides and bottom of the domain.

[18] The simulations were performed using the volume of fluid (VOF) multiphase model, which allowed us to simulate the air-sea interface including surface tension at the water surface. The surface tension coefficient was set at 0.072 N m^{-1}. The large eddy simulation Wall-Adapting Local Eddy-Viscosity (WALE) turbulence model [*Nicoud and Ducros*, 1999] was used for all numerical experiments. In the rest of this section, we briefly describe the VOF and WALE models. More details can be found in *ANSYS, Inc.* [2009] and cited literature.

3.2. Volume of Fluid Multiphase Model

[19] The VOF formulation relies on the fact that the two fluids or phases are immiscible. VOF is, therefore, a suitable formulation for modeling processes at the interface between air and water. For better computational stability, the compressible phase (air) is selected as the primary phase.

[20] The VOF model solves a single set of momentum equations and tracks the volume fraction of water and air throughout the domain. In each control volume, the volume fractions of both phases obey the equation:

$$\alpha_a + \alpha_w = 1 \tag{8}$$

where α_a and α_w are the air and water volume fraction in the cell, respectively. Condition $\alpha_w = 1$ corresponds to a cell completely filled with water; while, condition $\alpha_w = 0$ corresponds to a cell completely filled with air. The cell contains the air-water interface when

$$0 < \alpha_w < 1. \tag{9}$$

The tracking of the interface between the air and water is accomplished by the solution of a continuity equation for the volume fraction of the secondary phase (water). This equation is as follows:

$$\rho_w^{-1}[\partial_t(\alpha_w\rho_w) + \nabla\cdot(\alpha_w\rho_w\vec{u})] = \rho_w^{-1}\left[\sum_{a=1}^{n}(\dot{m}_{aw} - \dot{m}_{wa})\right], \tag{10}$$

where $\vec{u}$ is the velocity field; $\dot{m}_{aw}$ is the mass transfer from air to water, and $\dot{m}_{wa}$ is the mass transfer from water to air. Equation (10) is solved for the secondary phase (water) through explicit time discretization:

$$\left(\alpha_w^{n+1}\rho_w^{n+1} - \alpha_w^n\rho_w^n\right) V/\Delta t + \sum_f \left(\rho_w U_f^n \alpha_{w,f}^n\right) = \left[\sum_{a=1}^{n}(\dot{m}_{aw} - \dot{m}_{wa})\right] V, \tag{11}$$

where $n+1$ is the index for the new (current) time step; n is the index for the previous time step, $\alpha_{w,f}$ is the face value of the water fraction (computed from the Geo-Reconstruct scheme); V is the volume of cell; U_f is the volume flux through the face, based on normal velocity. The primary-phase (air) volume fraction is computed from constraint equation (8).

[21] Convection and diffusion fluxes through the control volume faces (the second term on the left side of equation (11)) are computed and balanced with source terms within the control volume itself. The face fluxes near interfaces are

obtained using the geometric interface reconstruction scheme (Geo-Reconstruct scheme). The Geo-Reconstruct scheme is applied when the cell is near an interface between two phases (i.e., the cell is not completely filled with one phase). This scheme, as implemented in ANSYS Fluent, uses a piecewise-linear interpolation and involves the following three successive steps: 1) Calculation of the linear interface position relative to the center of each partially filled cell, which is based on information about the volume fraction and its derivatives in the cell; 2) Calculation of the advecting amount of fluid through each face using the computed linear interface representation and information about the normal and tangential velocity distribution on the face; 3) Calculation of the volume fraction in each cell using the balance of fluxes computed during step two.

[22] In the VOF formulation, the velocity field is obtained by solving a single momentum equation throughout the model domain [*ANSYS, Inc.*, 2009]:

$$\partial_t(\rho\vec{u}) + \nabla\cdot(\rho\vec{u}\vec{u}) = -\nabla p + \nabla\cdot\left[\mu\left(\nabla\vec{u} + \nabla\vec{u}^T\right)\right] + \rho g + \vec{F}_\sigma, \tag{12}$$

where the mixture density ρ and dynamic viscosity μ are defined as follows: $\rho = \alpha_w\rho_w + \alpha_a\rho_a$ and $\mu = \alpha_w\mu_w + \alpha_a\mu_a$. Equation (12) is dependent on the volume fractions of both water and air through the properties of density and viscosity. The calculated velocity field $\vec{u}$ is shared between the water and air phases. In the ANSYS Fluent implementation, a viscosity ratio exceeding 10^3 may lead to convergence difficulties. However, in the case of the air-water interface, this ratio is limited from above by 10^2.

[23] The external force $\vec{F}_\sigma$ in equation (12) is the surface tension force at the air-water interface. Following *Brackbill et al.* [1992], the surface tension force $\vec{F}_\sigma$ at the air-water interface is defined as follows:

$$\vec{F}_\sigma = 2\sigma\rho k_w\nabla a_w/(\rho_w + \rho_a), \tag{13}$$

where $k_w = \nabla\cdot(\nabla a_w/|\nabla a_w|)$. This surface tension force model alleviates topology constraints on modeling interfaces having surface tension without sacrificing accuracy. This model appears to be well suited for modeling the two-phase environment at the air-sea interface under hurricane conditions.

3.3. Subgrid-Scale Model

[24] We used large eddy simulation (LES) as the subgrid-scale model. LES resolves large scales directly, while subgrid scales are modeled [*Smagorinsky*, 1963; *Deardorff*, 1970]. Note that an alternative approach, direct numerical simulation (DNS), directly resolves the whole spectrum of turbulent scales. DNS, however, is not practical for the simulation of the disruption of the air-sea interface in the hurricane conditions. The critical importance of resolving the viscous sublayers at the air-sea interface would require using the molecular viscosity in the DNS simulation, which imposes severe Reynolds number limitation. LES also has limitations near interfaces, which, however, have been addressed by increasing the mesh resolution near the interface to 1 mm.

[25] The wall-adapting local Eddy-Viscosity (WALE) turbulence model [*Nicoud and Ducros*, 1999], which is used in our simulations, returns the correct wall asymptotic behavior for interface flows. WALE parameterizes the turbulent viscosity as follows:

$$\mu_t = \rho L_s^2\left(S_{ij}^d S_{ij}^d\right)^{3/2} \Big/ \left[\left(\bar{S}_{ij}\bar{S}_{ij}\right)^{5/2} + \left(S_{ij}^d S_{ij}^d\right)^{5/4}\right], \tag{14}$$

where $L_s = \min(\kappa d,\ c_w V^{1/3})$, $S_{ij}^d = 1/2\left(\bar{g}_{ij}^2 + \bar{g}_{ji}^2\right) - 1/3\,\delta_{ij}\bar{g}_{kk}^2$, and $\bar{g}_{ij} = \partial\bar{u}_i/\partial x_j$. Here L_s is the mixing length for subgrid scales, $\kappa = 0.4$ (von Kármán constant), d is the distance closest to the wall, and V is the volume of the computational cell. The constant c_w was set to the default value of $c_w = 0.325$.

[26] Additional subgrid scale terms are produced by the filtering of the surface tension and convection terms in the transport equation (12), which involve correlations of the sub-grid fluctuations of the phase-fraction, density, and surface tension [*Befrui et al.*, 2012]. These additional terms are neglected in the Volume-of-Fluid Large-Eddy-Simulation (VOF-LES) method in the absence of mathematical closure models. In fact, *de Villiers et al.* [2004] have shown that with relatively fine mesh resolution it is deemed acceptable to neglect these additional subgrid scale influences. This approach has been under development and verification for the jet break up process and atomization of non-reactive fluids in application to combustion and liquid rocket engines [*Corbinelli et al.*, 2010; *Befrui et al.*, 2012]. The modeling results of these authors have been validated with experimental data and shown good qualitative and quantitative accuracy for prediction of the KH interface instability waves and the liquid-sheet breakup process. The range of fluid velocities in the combustion and rocket engines is typically from 30 m s^{-1} to 300 m s^{-1}, which covers, and even exceeds, the range of the wind speeds observed in hurricanes. This suggests that the VOF-LES method offers a computational capability to aid development of fundamental knowledge of the air-sea interface breakup process in hurricane conditions.

[27] However, higher mesh resolution is required in order to explicitly resolve the full spectrum of air bubbles and spray droplets produced in the process of direct disruption of the air-sea interface by hurricane force winds. With a domain size relevant to the problem of the air-sea interface it is not feasible to perform numerical simulations down to micrometer scales. We therefore limit our quantitative analysis to average characteristics of the velocity and density fields, which appear to be well resolved by VOF-LES with the millimeter-scale grid resolution used in this work (see also discussion in *Corbinelli et al.* [2010]).

4. Simulation of the Air-Sea Interface Under Hurricane Conditions

[28] We have conducted numerical simulations to demonstrate the effects of direct disruption of the air-sea interface under hurricane force wind speed conditions using the model set up described in Section 3. For the case shown in Figure 2, the wind stress is 4 N m^{-2}. The wind stress is applied at the upper boundary of the air layer. The Koga number $K = 0.38$ calculated from equation (1) in this case

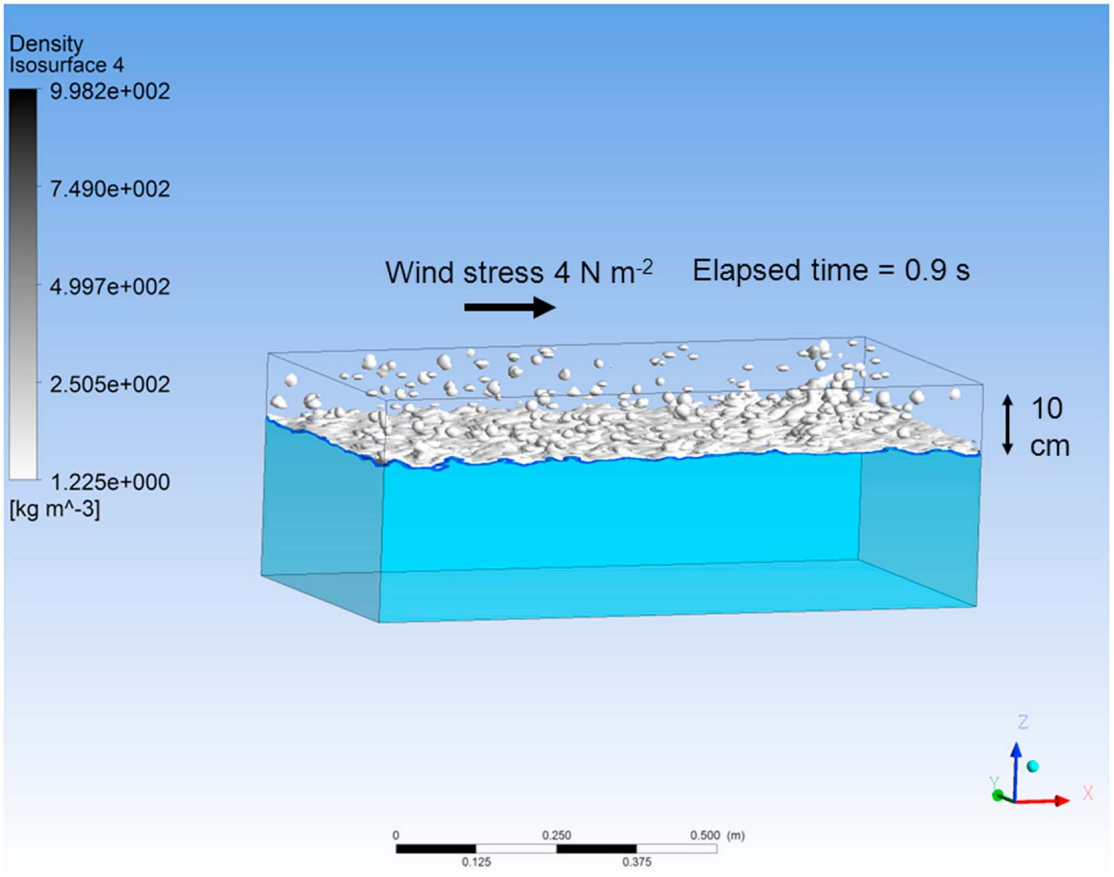

Figure 2. The numerical experiment with an initially flat interface illustrates the possibility of the direct disruption of the air-water interface and formation of the two-phase environment under hurricane force wind.

exceeds the critical value of K_{cr} = 0.26, which satisfies the condition for the development of the KH type instability, $K > K_{cr}$.

[29] The disruption of the air-water interface resembling the 'explosive' type instability and the formation of a two-phase environment are observed before any significant wind waves are able to develop. According to our simulation, the statistically stationary turbulent regime in the two-phase transitional layer establishes rapidly. The wind stress also generates surface waves, which have a much longer development cycle than turbulence in the two-phase layer. The turbulent part of the transitional layer eventually becomes undulated by developing surface waves. At that stage, the average vertical profiles in the turbulent portion of the transitional layer could therefore be affected ('blurred') by the wave motion that is not necessarily a turbulent type motion and, thus, does not characterize the turbulent component of the transitional layer. Furthermore, the presence of the wave component could affect Richardson number estimates from the average vertical profiles of density and velocity. Figure 2 shows the contour plot of density at the model time (t = 0.9 s) when turbulence in the two-phase layer has achieved a statistically stationary state but appreciable surface waves have not yet developed. At t = 0.9 s turbulence in the water layer below the transitional layer was not yet completely developed; however, the main action is concentrated on the air-side of the interface.

[30] It should be noted that the simulation of the full spectrum of air bubbles and spray droplets with this method would require a much increased mesh resolution, down to the micrometer range. The computational cost associated with such high mesh resolution would not be practical, even with the most powerful supercomputers.

[31] With the 1 mm vertical mesh resolution we are able to confidently resolve the two-phase transitional layer at the air-water interface, which is of approximately 2 cm thickness (Figure 3). In this case, the size distribution of drops and bubbles on unresolved scales (i.e., less than 1 mm) should not significantly affect the average profiles of density and velocity in the transitional layer, which is consistent with *de Villiers et al.* [2004] assumption accepted in the VOF-LES method that the sub-grid fluctuations of the phase-fraction, density, and surface tension, are all neglected in the VOF-LES method (see discussion at the end of Section 3).

[32] The averaged density and velocity profiles over the entire model domain excluding 0.2 m from each boundary in the *x*-direction and 0.05 m from each lateral boundary (*y*-direction) are shown in Figure 3. For the analysis of the results shown in Figure 3, we have used the following

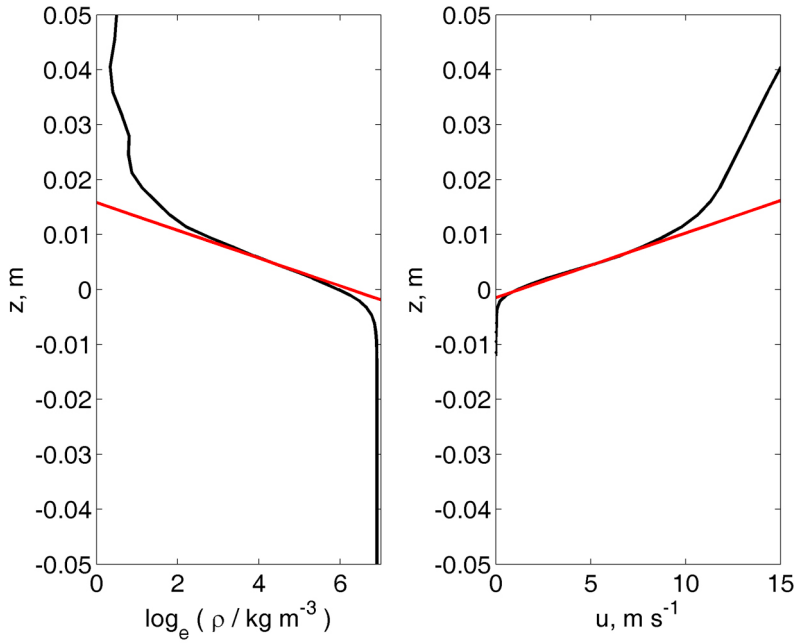

Figure 3. Averaged (left) vertical density and (right) velocity profiles at the air-sea interface for the case shown in Figure 2.

formulation for the local gradient Richardson number in the two-phase transition layer:

$$Ri = N^2/(\partial u/\partial z)^2 \tag{15}$$

where

$$N^2 = g\rho^{-1}\partial\rho/\partial z = g\partial(\log_e\rho)/\partial z = g\partial(\log_e\rho/\rho_a)/\partial z \tag{16}$$

is the squared Brunt–Väisälä frequency. We assume here unidirectional flow and ignore the average velocity component in the transverse direction. This form of the gradient Richardson number is applicable to large density differences as well. Respectively, the vertical profile of the density logarithm is plotted in Figure 3 (left). There is a linear segment on the logarithmic density profile in the transition layer. There is also a linear segment on the average velocity profile u in the transition layer (Figure 3, right).

[33] The linear segments on the vertical profiles shown in Figures 3 (left) and 3 (right) can be explained from the analysis of dimensions. The corresponding functional dependences are as follows:

$$\rho^{-1}\partial\rho/\partial z = \partial(\log_e\rho/\rho_a)/\partial z = function_\rho\left(g, u_*, \rho_a, \rho_w\right) \tag{17}$$

$$\partial u/\partial z = function_u\left(g, u_*, \rho_a, \rho_w\right) \tag{18}$$

The formal dimensional analysis [see, e.g., *Barenblatt*, 1996] results in the following dependences:

$$\partial(\log_e\rho/\rho_a)/\partial z = g u_*^{-2} F_\rho(\rho_a/\rho_w) \tag{19}$$

$$\partial u/\partial z = g u_*^{-1} F_u(\rho_a/\rho_w) \tag{20}$$

where F_ρ and F_u are universal dimensionless functions of dimensionless parameter ρ_a/ρ_w. Since $\rho_a/\rho_w \ll 1$, we assume the self-similarity on this parameter is achieved as an intermediate asymptotics [*Barenblatt*, 1996] in the range of densities determined by the inequality,

$$\rho_a \ll \rho \ll \rho_w. \tag{21}$$

Under the assumption of self-similarity, equations (19) and (20) transform as follows:

$$\partial(\log_e\rho/\rho_a)/\partial z = c_\rho g u_*^{-2}, \tag{22}$$

$$\partial u/\partial z = c_u g u_*^{-1}, \tag{23}$$

where c_ρ and c_u are dimensionless constants. Note that equations (22) and (23) describe linear dependences for $\log_e\rho$ and u on z, which are consistent with the presence of linear segments in the corresponding profiles in the transition layer in Figures 3 (left) and 3 (right). The linear dependences are based on the fact that among defining parameters there is no one with the length dimension. *Turner* [1973] applied similar considerations for gravity currents, which contained relatively small density differences, and derived linear dependences for the density and velocity profiles. Here, we apply similar considerations for the air-sea interface, which contains a very large density difference. For the case of a large density difference, instead of a linear profile for $\rho(z)$, a linear profile for $\log_e\rho(z)$ follows from the analysis of dimensions.

[34] Extrapolating the density profile in the two-phase transition layer, which is shown in Figure 3 (left), to the bulk air and water densities, we have obtained an estimate for the thickness of the transition layer as $H = 0.017$ m, which has

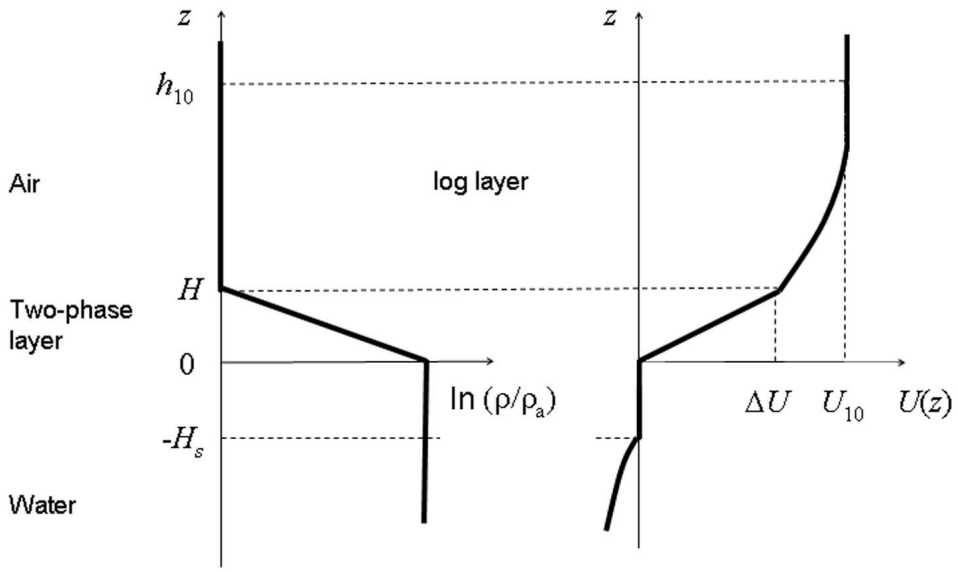

Figure 4. Schematic representation of density $\rho(z)$ and velocity $U(z)$ profiles in the atmospheric and oceanic boundary layers under hurricane conditions. Here: U_{10} is the wind speed at a standard measurement height h_{10} = 10 m; ΔU is the velocity difference across the two-phase transitional layer; H is the thickness of the transitional layer; H_s is the depth of wave-stirred layer. The density profile in the atmospheric boundary layer $z > H$ is assumed to obey the log layer law as well but is not shown on this diagram.

been found between $z_1 = -0.0016$ m and $z_2 = 0.0151$ m depths. The velocity difference in the corresponding layer in Figure 3 (right), as determined from extrapolation of the linear segment on the velocity profile to depths z_1 and z_2 corresponding to the schematics shown in Figure 4, is equal to $\Delta U = 15.3$ m s^{-1}. Entering these values in equations (5) has provided us with an estimate for the critical value of the global Richardson number, $Ri_{cr} = 0.257$, which is close to the theoretical value for three-dimensional flow of 1/4.

5. Parameterization for the Lower Limit of the Air-Sea Drag Coefficient Under Hurricane Conditions

[35] Figure 4 shows a schematic representation of the vertical structure of the two-phase transition layer based on the results of the numerical experiment. We have used these schematics in order to derive the dependence of the air-water drag coefficient C_{10} on wind speed U_{10}. For this purpose we have used a system of equations similar to *Soloviev and Lukas* [2010] but with a refinement for the formula describing the depth of the two-phase transition layer, H in equation (27):

$$U_{10} = u_{*a}\kappa^{-1}\log_e[(h_{10}+z_0)/z_0], \tag{24}$$

$$\Delta U = u_{*a}\kappa^{-1}\log_e[(H+z_0)/z_0], \tag{25}$$

$$u_{*a} = C_{10}{}^{1/2}U_{10}, \tag{26}$$

$$H = 2mRi_{cr}\Delta U^2\rho_a\rho_w\left(\rho_w^2-\rho_a^2\right)^{-1}g^{-1}, \tag{27}$$

$$z_0 = cH, \tag{28}$$

where U_{10} is the wind speed at a standard reference height h_{10} = 10 m, C_{10} is the drag coefficient, z_0 is the surface roughness length scale, c is the dimensionless coefficient connecting surface roughness length scale z_0 and thickness of the transition layer H, and κ is the von Kármán constant ($\kappa = 0.4$).

[36] Equations (24) and (25) are based on an assumption of the logarithmic wind speed profile in the atmospheric boundary layer above the transition layer. Relationship (26) is the formula for the friction velocity via the air-sea drag coefficient and wind speed at a 10 m level. Equation (27) is derived in section 2; this equation takes into account the presence of the logarithmic profile of wind speed above the transition layer. Equation (28) defines the surface roughness length as a proportional to the transition layer thickness with the proportionality coefficient c.

[37] Note that the origin of the coordinate system is taken here as the base of the transition layer, since most, but not all, of the velocity change takes place above the still water level. Moreover, the practical applications require estimation of drag coefficient with respect to the bulk water.

[38] The system of equations (24)–(28) has been reduced to a single transcendental equation for C_{10},

$$C_{10} = \kappa^2\ln^{-2}\left\{1+h_{10}\left(2mRi_{cr}c\rho_a\rho_w(\rho_w-\rho_a)^{-1}g^{-1}\cdot C_{10}U_{10}{}^2\kappa^{-2}\ln^2\left(1+c^{-1}\right)\right)^{-1}\right\}, \tag{29}$$

and is solved numerically in MATLAB by an iteration method.

[39] The solution to equation (29) for C_{10} as a function of the wind speed U_{10} is shown in Figure 5 as the 'two-phase layer resistance' curve for $Ri_{cr} = 0.25$ (which was derived

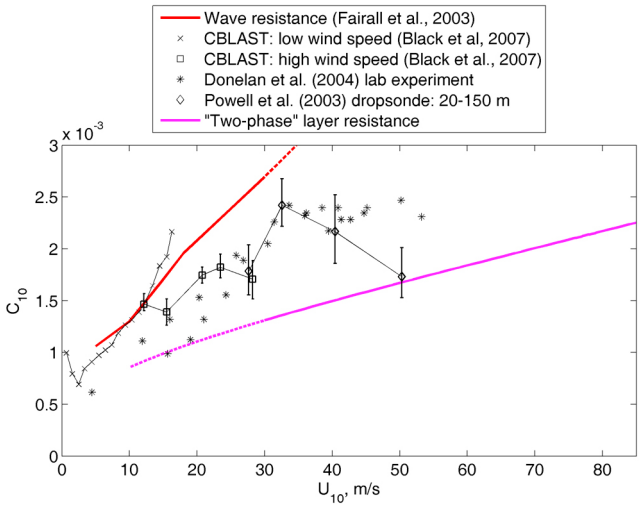

Figure 5. The two-phase layer and wave resistance parameterizations in comparison with available laboratory and field data.

from the numerical experiment). We have found that constants $c = 0.022$ and $m = 1$ provide a solution, which is consistent with the results obtained from the CFD simulation shown in Figure 3.

[40] The lower limit on the drag coefficient under hurricane conditions obtained by *Soloviev and Lukas* [2010] was represented by a range of curves due to some uncertainty in the values of dimensionless constants Ri_{cr}, c, and m. The parameterization derived in this work is represented by a single curve. This is a result of numerical experiments, which contributed to a better specification for the critical Richardson number Ri_{cr} and constants c and m. The new parameterization is, nevertheless, consistent with the uncertainty range reported in *Soloviev and Lukas* [2010].

[41] Laboratory data fall between the two-phase layer resistance parameterization from below and wave resistance parameterization from above (Figure 5). The field data also fall between these two parameterizations, which, however, are available only up to 50 m s^{-1} wind speed.

[42] Figure 6 shows the thickness of the two-phase transition layer H calculated from equations (24)–(27) versus wind speed, U_{10}. The thickness of the transition layer is relatively small, ranging from approximately 0.7 cm at U_{10} = 30 m s^{-1} to 10 cm at U_{10} = 85 m s^{-1}.

[43] The state of the sea surface in hurricane conditions varies in azimuth and distance from the hurricane center because of the variation in swell characteristics relative to the wind [*Powell et al.*, 2003; *Black et al.*, 2007]. The relative contribution of the wave and two-phase layer mechanisms to the drag coefficient is also expected to vary. In certain wind-wave interaction regimes, or because of suppression of short surface waves by the two-phase environment, the wave drag may become inefficient. In this case, the air-sea drag is due to the two-phase transition layer and the drag coefficient drops to its lower limit as indicated in Figure 5.

[44] As noticed in *Soloviev and Lukas* [2010] and evidently from Figure 5, the lower limit on the drag coefficient slowly increases with wind. This is because the two-phase transition layer takes a part of its momentum from the wind, which results in an increase of the drag coefficient with wind. *Andreas* [1998] anticipated a similar effect, considering additional resistance due to the transfer of a part of the wind momentum to the sea spray. Note that the role of sea spray in this process is to increase the air-sea drag coefficient rather to reduce it.

[45] *Soloviev and Lukas* [2006] estimated the Oboukhov buoyancy length scale L_B associated with the spray buoyancy flux. In the framework of the traditional formulation of the sea spray generation function [e.g., *Andreas*, 1998]: $L_B \gg h_{10}$. This suggests that the buoyancy flux associated with the entrainment of spray droplets in the airflow in hurricane conditions has a relatively small effect on the drag coefficient (C_{10}) when referred to a standard height, h_{10} = 10 m. *Ingel'* [2011] came to the similar conclusion that the intensity of spray production is probably insufficient to explain the air-sea drag saturation or reduction in hurricane conditions.

[46] At this point, the sea spray generation function is poorly known. Should the sea spray generation function be much larger, at least an order of magnitude, than its traditional formulation, the buoyancy flux due to sea spray would appreciably affect C_{10} [*Kudryavtsev and Makin*, 2011]. The buoyancy effect of the sea spray in hurricane conditions can, nevertheless, be appreciable at a height $h > L_B$, even with the existing sea spray generation function.

6. Numerical Experiments With Imposed Waves

[47] Development of a parameterization taking into account the impact of both wave and two-phase environment in

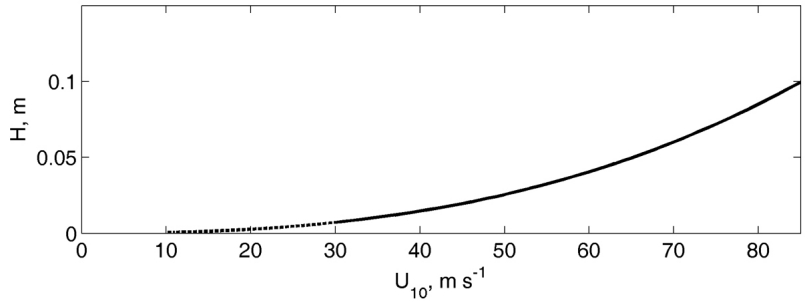

Figure 6. Thickness of the two-phase transitional layer.

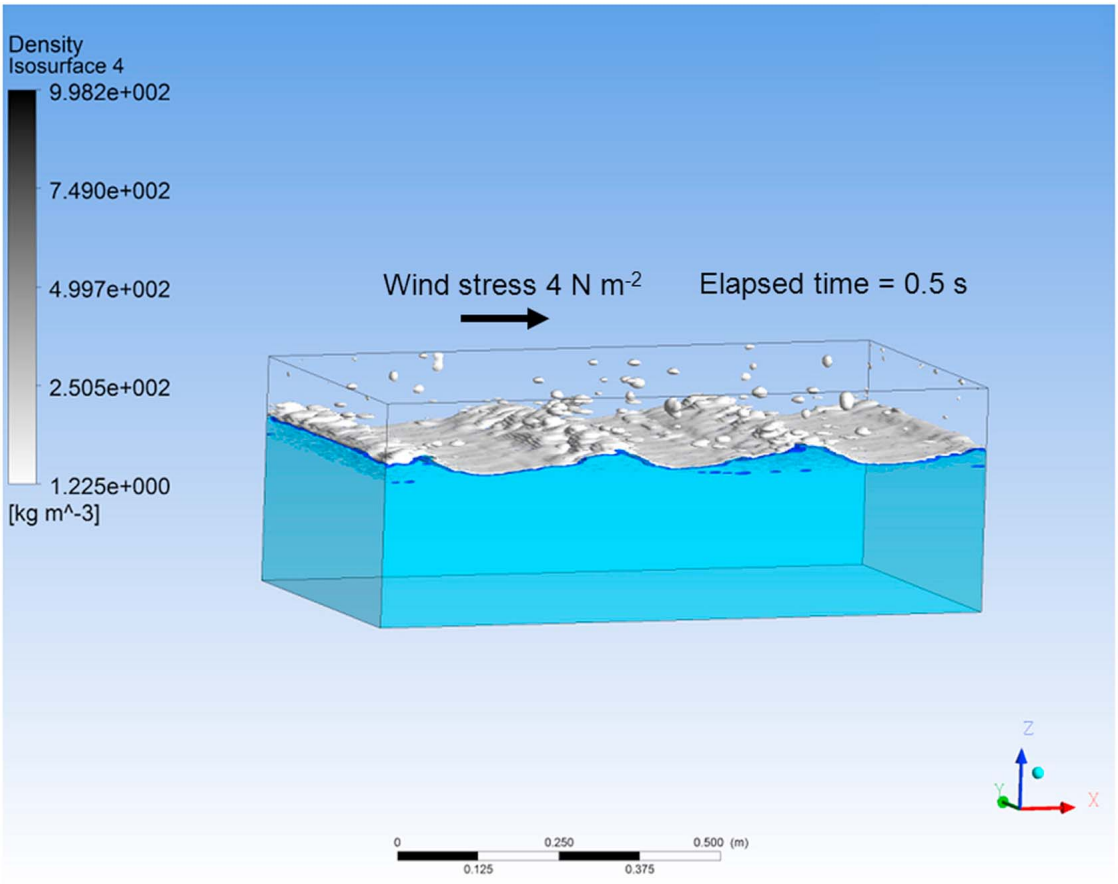

Figure 7. The numerical experiment with imposed short wavelets demonstrates the tearing of wave crests, formation of water sheets and spume ejection into the air.

the air-sea drag is important for the realistic representation of the air-sea interface in hurricane models. For this purpose, we conducted a series of numerical experiments aimed at understanding the basic mechanisms of wind wave interactions.

[48] The numerical experiments with imposed short waves demonstrated the tearing of wave crests, formation of water sheets and spume ejected into the air, and smoothing of the water surface in the direction of the airflow (Figure 7). There are also signatures of parasitic capillaries developing on the forward face of the waves. However, the full resolution of the parasitic capillaries would require better mesh resolution in the horizontal direction [*Tsai and Hung*, 2007].

[49] Figure 8 shows a different view on the surface, which reveals intermittent streamwise structures with periodicity in the transverse direction on the top of wavelets. The numerical simulation reveals formation of streamwise coherent structures on the water surface in the form of streaks of spanwise size on the order of a few cm. The streaks observed in Figure 8 could be a result of the TS instability. According to *McNaughton and Brunet* [2002], the nonlinear stage of the TS instability results in streamwise streaks followed by fluid ejections. This mechanism can contribute to the generation of spume in the form of streaks. Similar streak-like structures have previously been reported from experiments and numerical simulations near the rigid wall [*Lesieur*, 2008] and below the free surface [*Dhanak and Si*, 1999; *Tsai*, 2001].

[50] According to *Lesieur* [2008], the streaks near the rigid wall are of spanwise size $\sim 10d$, where

$$d \approx 10\nu/u_{*w} \tag{30}$$

is the thickness of the viscous sublayer, ν is the water viscosity, $u_{*w} = (\tau_t/\rho_w)^{1/2}$, and τ_t is the skin-stress. Under hurricane force winds, a significant portion of wind stress goes to the wave momentum. Assuming that in this case the skin-stress is represented only by a few percent of the wind stress, the corresponding spanwise size of the streaks is of the order of a few cm, which is consistent with the modeling results shown in Figure 8.

[51] Foam streaks are an observable feature on photographic images of the ocean surface under hurricane conditions (Figure 9). At this point, however, it is difficult to conclude if the coherent structures observed in the numerical experiment and in the ocean are of the same nature, since our numerical model operates in a much smaller domain compared to the photo images of the sea surface shown in Figure 9. However, the spanwise size of streaks in this case can be scaled with the depth of the wave-stirred layer. According to *Soloviev and Lukas* [2003], the depth of the wave-stirred layer is $\sim 0.2H$, where H is the significant wave

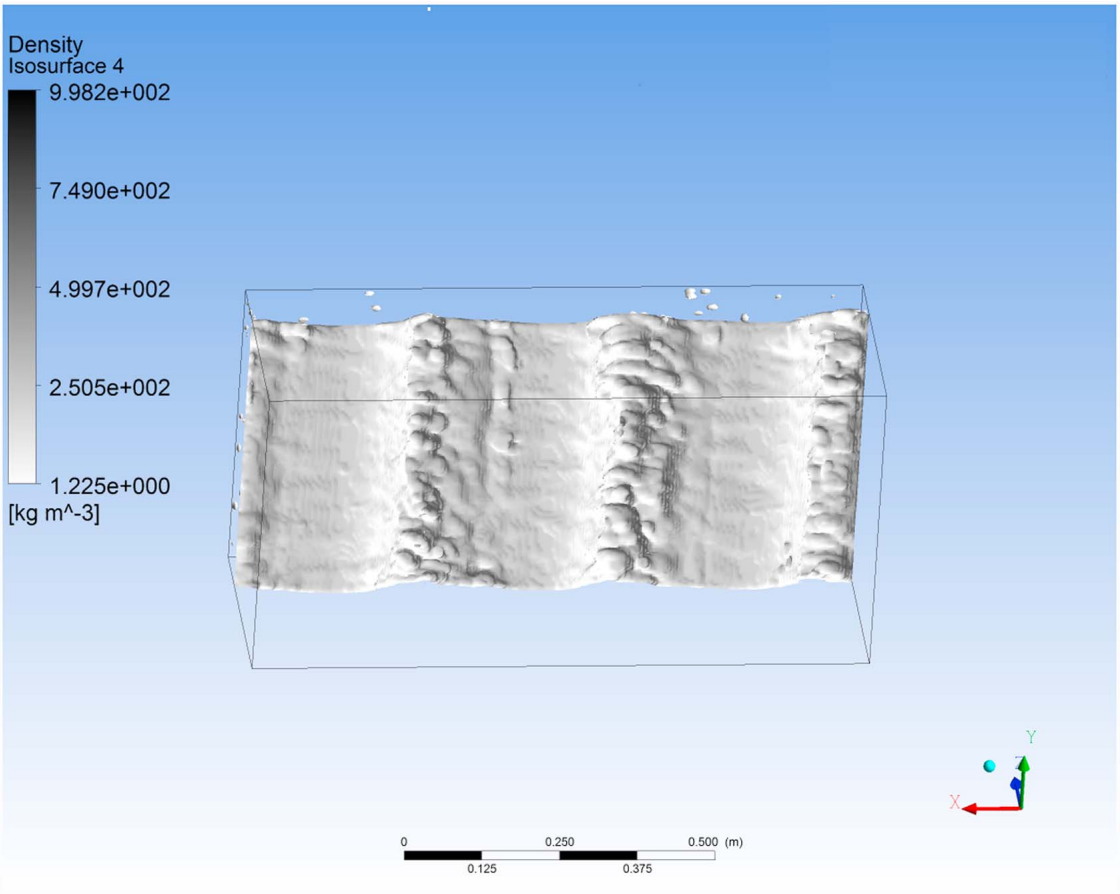

Figure 8. View on the air-water surface to demonstrate quasiperiodic structures in the transverse direction on the top of wave crests.

height. For H = 10 m, the *Lesieur* [2008] type scaling hence results in the spanwise size of streaks of the order of 20 m, which is consistent with the streaks observed in Figure 9.

[52] It should be noted that for the break-up of the air-water interface by the KH waves, pressure fluctuation due to the form drag are important [*Hoepffner et al.*, 2011]. On the other hand, the TS instability develops in viscous sublayers and is driven by the skin component of the wind stress.

7. Discussion and Conclusions

[53] The effects of direct disruption of the air-sea interface and formation of a two-phase transitional layer have been

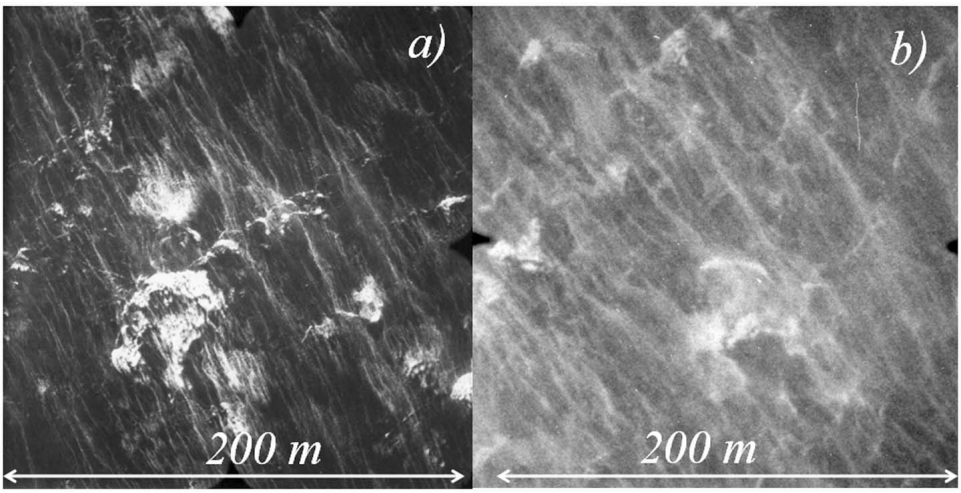

Figure 9. Ocean surface foam streaks observed on photographic images of the sea surface in a hurricane: (a) wind speed 28 m s^{-1} and (b) wind speed 46 m s^{-1} [after *Black et al.*, 2006].

simulated with a high-resolution numerical model. The VOF-LES multiphase model included surface tension at the water-air interface. The model was initialized with either a flat interface or short wavelets. Wind stress was applied at the upper boundary of the air layer, ranging from zero stress to hurricane force stress in different experiments. The direct disruption of the air-water interface and formation of the two-phase transition layer were observed in the numerical model under hurricane force wind. This was consistent with the Koga number criteria, $K > K_{cr} \approx 0.26$. The mechanism of the interface disruption resembled the Kelvin-Helmholtz type instability.

[54] The direct disruption of the air-water interface results in the formation of a two-phase environment and a transition layer between water and air. The air-water interface is no longer explicitly identifiable. As a consequence, the analysis of dimensions suggests linear dependences for $\log_e \rho(z)$ and $u(z)$ on z. The numerical simulations confirmed the presence of linear segments in the corresponding profiles within the transition layer. Such vertical profiles of density and velocity in the transition layer were consistent with the regime of marginal stability, which permitted a parameterization of the equivalent drag coefficient caused by the presence of the two-phase transition layer at the air-sea interface. This parameterization represents the lower limit imposed on the drag coefficient under hurricane conditions. This limit is appreciably lower than the wave resistance law; though, it gradually increases with wind speed. The numerical simulations helped to reduce the uncertainty in the critical Richardson number applicable to the air-sea interface and in the values of two dimensionless constants, which reduced the uncertainty in the parameterization of the lower limit on the drag coefficient. The available laboratory and field data fall between the two-phase layer parameterization from below and wave resistance parameterization from above.

[55] Both wave and two-phase environment contribute to the momentum transfer at the air-sea interface. For realistic representation of the air-sea interface in hurricane models it is necessary to account for both wave and two-phase environment contribution in the momentum transfer. For this purpose, we conducted a series of numerical experiments aimed at understanding of basic mechanisms of wind-wave interaction. The experiments with imposed short wavelets demonstrated the tearing of wave crests, formation of water sheets, spume ejection into the air, and smoothing of the water surface. Streamwise coherent structures observed on the water surface, especially prominent on the top of wave crests, resembled the Tollmien-Schlichting instability. This suggests that a similar process at the air-sea interface might be a cause of the foam streaks, which are observed on the ocean surface under hurricane conditions from the hurricane hunter airplanes.

[56] High-resolution numerical simulations using CFD appear to be an effective tool for improving our understanding of the complex processes taking place at the air-sea interface under high wind speed conditions. The results presented in this work are expected to help in developing a conceptual framework for merging the effects of the two-phase environment with the contribution to the drag from waves.

[57] In this research, we have capitalized on significant development and success of VOF-LES methods for simulation of the atomization process in non-reactive fluid jets in engineering applications. The range of fluid velocities in these applications is from 30 m s^{-1} to 300 m s^{-1}, which covers, and even exceeds, the range of the wind speeds observed in hurricanes. These methods have been implemented in the commercial software ANSYS Fluent and validated in a number of laboratory experiments. Application of CFD to the problem of the air-sea interface in hurricane conditions, however, involves a wider range of spatial scales than typical engineering applications. Validation of these methods at air-sea interaction facilities and, possibly, in nature, in the presence of a spectrum of surface waves, is therefore an important though challenging subject of future research.

[58] **Acknowledgments.** The authors are grateful to Roger Lukas (UH), Isaac Ginis and Tetsu Hara (URI), Shuyi Chen, Brian Haus, and Mark Donelan (UM RSMAS), and Vladimir Kudryavtsev (NERSC) for important discussions of the problem. We thank Mikhail Gilman (NCSU) for help with numerical modeling and Jenny Fenton (NSUOC) for technical help in the preparation of the manuscript. We also thank anonymous reviewers for valuable comments. We acknowledge support from the NSUOC project "Hydrodynamics and remote sensing of far wakes of ships," the NOPP project "Advanced coupled atmosphere-wave-ocean modeling for improving tropical cyclone prediction models" (PIs: Isaac Ginis and Shuyi Chen), and GoMRI project "Consortium for advanced research on transport of hydrocarbon in the environment" (PI: Tamay M. Özgökmen).

References

Andreas, E. L. (1998), A new sea spray generation function for wind speeds up to 32 m s^{-1}, *J. Phys. Oceanogr.*, *28*, 2175–2184, doi:10.1175/1520-0485(1998)028<2175:ANSSGF>2.0.CO;2.

ANSYS, Inc. (2009), *ANSYS FLUENT 12.0 Theory Guide*, Canonsburg, Pa.

Babanin, A. V., and B. K. Haus (2009), On the existence of water turbulence induced by non-breaking surface waves, *J. Phys. Oceanogr.*, *39*(10), 2675–2679, doi:10.1175/2009JPO4202.1.

Barenblatt, G. I. (1996), *Scaling, Self-Similarity, and Intermediate Asymptotics*, 386 pp., Cambridge Univ. Press, Cambridge, U. K.

Befrui, B., G. Corbinelli, P. Spiekermann, M. Shost, and M. C. Lai (2012), Large eddy simulation of GDI single-hole flow and near-field spray, *SAE Int. J. Fuels Lubr.*, *5*(2), 620–636, doi:10.4271/2012-01-0392.

Black, P. G., E. Uhlhorn, A. Goldstein, I. Popstefanija, and J. Carswell (2006), SFMR performance during the 2005 hurricane season, paper presented at 60th Interdepartmental Hurricane Conference, Off. of the Fed. Coord. for Meteorol. Serv. and Supporting Res., Mobile, Ala., 20–24 March. [Available at http://www.ofcm.gov/ihc06/Presentations/Posters/p-03-black-POSTER-IHC06_SFMR.pdf.]

Black, P. G., E. A. D'Asaro, W. M. Drennan, J. R. French, P. P. Niiler, T. B. Sanford, E. J. Terrill, E. J. Walsh, and J. A. Zhang (2007), Air-sea exchange in hurricanes: Synthesis of observations from the Coupled Boundary Layer Air-Sea Transfer experiment, *Bull. Am. Meteorol. Soc.*, *88*(3), 357–374, doi:10.1175/BAMS-88-3-357.

Brackbill, J. U., D. B. Kothe, and C. Zemach (1992), A continuum method for modeling surface tension, *J. Comput. Phys.*, *100*, 335–354, doi:10.1016/0021-9991(92)90240-Y.

Corbinelli, G., B. Befrui, and W. Reckers (2010), Large eddy simulation and optical studies of the primary break-up of a thin planar-sheet liquid jet, *SAE Int. J. Fuels Lubr.*, *3*(1), 266–276, doi:10.4271/2010-01-0622.

Cushman-Roisin, B. (1994), *Introduction to Geophysical Fluid Dynamics*, 290 pp., Prentice Hall, Englewood Cliffs, N. J.

Cushman-Roisin, B., and J.-M. Beckers (2011), *Introduction to Geophysical Fluid Dynamics. Physical and Numerical Aspects*, 875 pp., Academic, San Diego, Calif.

Deardorff, J. (1970), A numerical study of three-dimensional turbulent channel flow at large Reynolds numbers, *J. Fluid Mech.*, *41*(02), 453–480, doi:10.1017/S0022112070000691.

de Villiers, E., A. Gosman, and H. Weller (2004), Large eddy simulation of primary diesel spray atomization, *SAE Tech. Pap. 2004-01-0100*, SAE Int., Warrendale, Pa., doi:10.4271/2004-01-0100.

Dhanak, M. R., and C. Si (1999), On reduction of turbulent wall friction through spanwise wall oscillations, *J. Fluid Mech.*, *383*, 175–195, doi:10.1017/S0022112098003784.

Donelan, M. A., B. K. Haus, N. Reul, W. Plant, M. Stiassnie, H. Graber, O. Brown, and E. Saltzman (2004), On the limiting aerodynamic roughness of the ocean in very strong winds, *Geophys. Res. Lett.*, *31*, L18306, doi:10.1029/2004GL019460.

Fairall, C. W., E. F. Bradley, J. E. Hare, A. A. Grachev, and J. B. Edson (2003), Bulk parameterization of air-sea fluxes: Updates and verification for the COARE algorithm, *J. Clim.*, *16*, 571–591, doi:10.1175/1520-0442(2003)016<0571:BPOASF>2.0.CO;2.

Fan, Y., I. Ginis, and T. Hara (2009), The effect of wind-wave-current interaction on air-sea momentum fluxes and ocean response in tropical cyclones, *J. Phys. Oceanogr.*, *39*, 1019–1034, doi:10.1175/2008JPO4066.1.

Gramer, L. (2007), Kelvin-Helmholtz Instabilities: GFD-II, report, 32 pp., Univ. of Miami, Miami, Fla.

Hoepffner J., R. Blumenthal, and S. Zaleski (2011), Self-similar wave produced by local perturbation of the Kelvin-Helmholtz shear-layer instability, *Phys. Rev. Lett.*, *106*(10), 104502, doi:10.1103/PhysRevLett.106.104502.

Ingel', L. K. (2011), On the effect of seas spray on the dynamics of the marine atmospheric layer in strong winds, *Izv. Russ. Acad. Sci. Atmos. Oceanic Phys.*, Engl. Transl., *47*(1), 119–127, doi:10.1134/S0001433811010099.

Koga, M. (1981), Direct production of droplets from breaking wind-waves—Its observation by a multi-colored overlapping exposure technique, *Tellus, Ser. A*, *33*, 552–563, doi:10.1111/j.2153-3490.1981.tb01781.x.

Kudryavtsev, V. N., and V. K. Makin (2011), Impact of ocean spray on the dynamics of the marine atmospheric boundary layer, *Boundary Layer Meteorol.*, *140*, 383–410, doi:10.1007/s10546-011-9624-2.

Kukulka, T., and T. Hara (2008), The effect of breaking waves on a coupled model of wind and ocean surface waves. Part II: Growing seas, *J. Phys. Oceanogr.*, *38*, 2164–2184, doi:10.1175/2008JPO3962.1.

Kukulka, T., T. Hara, and S. E. Belcher (2007), A model of the air-sea momentum flux and breaking-wave distribution for strongly forced wind waves, *J. Phys. Oceanogr.*, *37*, 1811–1828, doi:10.1175/JPO3084.1.

Lasheras, J. C., and E. J. Hopfinger (2000), Liquid jet instability and atomization in a coaxial jet stream, *Annu. Rev. Fluid Mech.*, *32*, 275–308, doi:10.1146/annurev.fluid.32.1.275.

Lefebvre, A. H. (1989), *Atomization and Spray*, 421 pp., Hemisphere, New York.

Lesieur, M. (2008), *Turbulence in Fluids*, 4th ed., 148 pp., Springer, New York.

McNaughton, K. G., and Y. Brunet (2002), Townsend's hypothesis, coherent structures and Monin-Obukhov similarity, *Boundary Layer Meteorol.*, *102*, 161–175, doi:10.1023/A:1013171312407.

Miles, J. W., and L. N. Howard (1964), Note on a heterogeneous shear flow, *J. Fluid Mech.*, *20*, 331–336, doi:10.1017/S0022112064001252.

Nicoud, F., and F. Ducros (1999), Subgrid-scale stress modelling based on the square of the velocity gradient tensor, *Flow Turbul. Combust.*, *62*, 183–200, doi:10.1023/A:1009995426001.

Powell, M. D., P. J. Vickery, and T. A. Reinhold (2003), Reduced drag coefficient for high wind speeds in tropical cyclones, *Nature*, *422*, 279–283, doi:10.1038/nature01481.

Qiao, F., Y. Yuan, T. Ezer, C. Xia, Y. Yang, X. Lu, and Z. Song (2010), A three-dimensional surface wave-ocean circulation coupled model and its initial testing, *Ocean Dyn.*, *60*(5), 1339–1355, doi:10.1007/s10236-010-0326-y.

Smagorinsky, J. (1963), General circulation experiments with the primitive equations, *Mon. Weather Rev.*, *91*(3), 99–164, doi:10.1175/1520-0493(1963)091<0099:GCEWTP>2.3.CO;2.

Soloviev, A., and R. Lukas (2003), Observation of wave enhanced turbulence in the near surface layer of the ocean during TOGA COARE, *Deep Sea Res., Part I*, *50*, 371–395, doi:10.1016/S0967-0637(03)00004-9.

Soloviev, A., and R. Lukas (2006), *The Near-Surface Layer of the Ocean: Structure, Dynamics, and Applications*, 572 pp., Springer, Dordrecht, Netherlands.

Soloviev, A., and R. Lukas (2010), Effects of bubbles and spray on air-sea exchange in hurricane conditions, *Boundary Layer Meteorol.*, *136*, 365–376, doi:10.1007/s10546-010-9505-0.

Troitskaya, Y., V. Kazakov, N. Bogatov, O. Ermakova, M. Salin, D. Sergeev, and M. Vdovin (2010), Laboratory investigation of wind-wave interaction under severe wind conditions, paper presented at 29th Conference on Hurricanes and Tropical Meteorology, Am. Meteorol. Soc., Tucson, Arizona, 10–14 May.

Tsai, W. (2001), On the formation of streaks on wind-driven water surfaces, *Geophys. Res. Lett.*, *28*(20), 3959–3962, doi:10.1029/2001GL013190.

Tsai, W.-T., and L.-P. Hung (2007), Three-dimensional modeling of small-scale processes in the upper boundary layer bounded by a dynamic ocean surface, *J. Geophys. Res.*, *112*, C02019, doi:10.1029/2006JC003686.

Turner, J. S. (1973), *Buoyancy Effects in Fluids*, 382 pp., Cambridge Univ. Press, New York, doi:10.1017/CBO9780511608827.

Wang, G., and F. Qiao (2008), Ocean temperature responses to typhoon Mstsa in the East China Sea, *Acta Oceanol. Sin.*, *27*(4), 26–38.

Yecko, P., S. Zaleski, and J.-M. Fullana (2002), Viscous modes in two-phase mixing layers, *Phys. Fluids*, *14*(12), 4115–4122, doi:10.1063/1.1513987.